PROCEEDINGS

55. IWK

Internationales Wissenschaftliches Kolloquium
International Scientific Colloquium

13 - 17 September 2010

Crossing Borders within the ABC

Automation,

Biomedical Engineering and

Computer Science

Faculty of
Computer Science and Automation

www.tu-ilmenau.de

TECHNISCHE UNIVERSITÄT
ILMENAU

Impressum
Published by

Publisher:	Rector of the Ilmenau University of Technology Univ.-Prof. Dr. rer. nat. habil. Dr. h. c. Prof. h. c. Peter Scharff
Editor:	Marketing Department (Phone: +49 3677 69-2520) Andrea Schneider (conferences@tu-ilmenau.de) Faculty of Computer Science and Automation (Phone: +49 3677 69-2860) Univ.-Prof. Dr.-Ing. habil. Jens Haueisen
Editorial Deadline:	20. August 2010
Implementation:	Ilmenau University of Technology Felix Böckelmann Philipp Schmidt

USB-Flash-Version.

Publishing House:	Verlag ISLE, Betriebsstätte des ISLE e.V. Werner-von-Siemens-Str. 16 98693 Ilmenau
Production:	CDA Datenträger Albrechts GmbH, 98529 Suhl/Albrechts
Order trough:	Marketing Department (+49 3677 69-2520) Andrea Schneider (conferences@tu-ilmenau.de)

ISBN: 978-3-938843-53-6 (USB-Flash Version)

Online-Version:

Publisher:	Universitätsbibliothek Ilmenau ilmedia Postfach 10 05 65 98684 Ilmenau

Home / Index:
http://www.db-thueringen.de/servlets/DocumentServlet?id=16739

A NEW SEGMENTATION ALGORITHM FOR LOW CONTRAST POSITRON EMISSION TOMOGRAPHY BASED ON ANT COLONY OPTIMIZATION

Haase R[1,2], Hietschold V[2,3], Andreeff M[4], Böhme H-J[1], Abolmaali N[2,3]

[1] Faculty of Information Technology / Mathematics, University of Applied Sciences Dresden,
[2] OncoRay, Center for Radiation Research in Oncology, Medical Faculty Carl Gustav Carus, TU Dresden,
[3] Institute and Policlinic for Diagnostic Radiology, University Clinic Carl Gustav Carus, TU Dresden,
[4] Clinic for Nuclear Medicine, University Clinic Carl Gustav Carus, TU Dresden

ABSTRACT

In modern oncology, non-invasive imaging of aspects of tumour biology has a growing importance. One issue is tumour hypoxia imaging, for example with positron emission tomography (PET) using the tracer [^{18}F]-fluoromisonidazole (FMISO). But FMISO-PET datasets usually show a low target to background contrast. So the exact delineation of the hypoxic volume is typically done manually and challenging, even for experienced oncologists. For this purpose we propose a fully automatic segmentation algorithm. Our approach is based on the ant colony optimization (ACO) meta-heuristic, combined with thresholding the pheromone field, which is generated by virtual ants exploring the PET dataset. The results indicate that the approach can be successfully applied to segment PET phantom datasets with low contrast. Further development of the method seems worthwhile to segment patient data sets, for example to assist radio therapy planning.

Index Terms – Positron Emission Tomography, Ant Colony Optimization, Image Segmentation, Thresholding

1. INTRODUCTION

In modern oncology a wide range of non-invasive imaging techniques gain interest of both, scientists and physicians. An important aspect of tumour biology imaging is detection and localisation of hypoxic regions inside a cancerous volume. On the one hand, measuring tumour hypoxia might allow therapy prognosis and on the other hand it could be included into making therapeutic decisions. Especially in radiation therapy the knowledge of present tumour hypoxia is needed to improve therapy response, because hypoxic cells show increased radioresistance. While positron emission tomography (PET) using the tracer [^{18}F]-fluoromisonidazole (FMISO) already showed its applicability for hypoxia imaging [1], it has not yet been introduced in clinical routine. There are two main issues to enhance FMISO-PET to an applicable imaging technique for answering oncological questions. The first one is the limited reproducibility caused by biological and technological aspects [2]. The second issue is, that in comparison with an established tracer, like [^{18}F]-fluorodeoxyglucose (FDG), FMISO-PET shows very low contrast. A pair of FMISO- and FDG-PET images from a head and neck cancer patient is exemplary shown in figure 1. The low contrast interferes standard segmentation algorithms. An alternative approach is strongly needed. Nature inspired heuristics, like the Ant-Colony-Optimization (ACO) method, are able to achieve good solutions for a wide range of complex tasks [3]. ACO was introduced by [4] and recently applied to medical image segmentation [5], more precisely to the segmentation of Magnetic Resonance Images. Developing a segmentation algorithm based on ACO for three dimensional low contrast PET data sets is in the focus of this paper.

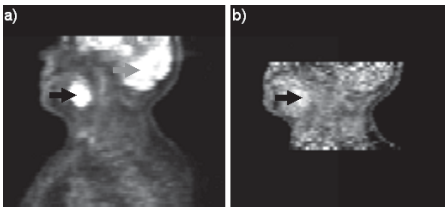

Figure 1: The comparison of two different PET data sets shows differences in contrast. a) FDG-PET of a patient with a region of high signal indicates a tumour near the base of the tongue (black arrow). The cerebellum also shows high signal (grey arrow). b) FMISO-PET of the same patient acquired four days after FDG-PET. High signal inside tumour volume (black arrow) suggests the presence of hypoxic cells.

2. METHODS AND MATERIALS

2.1. Measuring contrast and segmentation quality

To measure the contrast of the PET data sets the maximum activity A_t inside a defined target volume, the mean activity A_{bg} and the standard deviation σ_{bg} of

a defined background region are measured. These measurements lead to the contrast-to-noise-ratio CNR_{max}:

$$CNR_{max} = (A_t - A_{bg}) / \sigma_{bg}$$

To measure segmentation quality, three key figures are calculated: Jaccard-Index, sensitivity and specificity. The Jaccard-Index, a measure of congruence in the theory of sets, is calculated by considering positive voxels as sets. All positive classified voxels inside a data set are considered as set A and all positive voxels in the reference volume are considered as set B. The Jaccard-Index J of these two sets is defined as the ratio between intersection and union of A and B:

$$J(A, B) = |A \cap B| / |A \cup B|$$

Comparison of the resulting classification of all voxels and a binary reference allows separating all positive classified voxels into the categories true positive (tp) and false positive (fp), all negative voxels are separated into true negative (tn) and false negative (fn). The amount n of these voxel categories leads to the definition of sensitivity SE and specificity SP:

$$SE = P(p|tp) = n_{tp} / (n_{tp} + n_{fn})$$

$$SP = P(n|tn) = n_{tn} / (n_{tn} + n_{fp})$$

2.2. Experimental phantom

To get a wide range of differently contrasted data sets phantom experiments were performed. The phantom is comprised of a cylinder containing a solution of [^{18}F]-Fluorine and inside the cylinder six spheres. Two of them are spherical shells filled with a solution containing [^{68}Ga]-Gallium, the other four are wax spheres partly consisting of [^{68}G]-Gallium. The six spheres served as target objects. The volume inside the cylinder was considered as background activity, a simplification of surrounding normal tissue in patient data sets near the target volume. Using two different isotopes for target and background lead to falling contrast with time, because of the different half life of the used radio nuclides. With a waiting period of 10 minutes 63 data sets of the phantom were acquired using a clinical PET-CT Scanner (Siemens Biograph 16). To get an alternative view on the target objects, an additional CT data set of the phantom was acquired. CT and PET where fused to delineate the target objects manually. This delineation was transformed to a binary dataset as reference for evaluating the segmentation algorithm. One slice of the CT image stack, the binary reference, and a corresponding slice of a PET data set of the phantom are shown in figure 2.

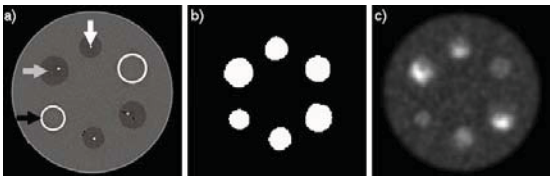

Figure 2: Slice images of the three-dimensional volumes acquired from phantom experiments. a) CT dataset with glass spheres (black arrow) and wax spheres (grey arrow) fixed on a metal wire (white arrow). b) The binary data set shows membership of voxels to the target objects (white). c) PET dataset

2.3. Simulated phantom

Phantom simulations programmed in the Interactive Data Language (ITT Visual Information Solutions) admit testing the segmentation algorithm under various conditions. The simulation generated volumes with a cylinder and six spheres with varying mean activity, to imitate the experimental phantom data sets. A three dimensional Gaussian filter was applied to the volumes to simulate the mean flight distance of the positrons as well as properties of the PET image reconstruction algorithm. Noise was added to the data sets by randomization of the grey values of the voxels with a Poisson distribution. The simulation required two parameters, the mean background activity and the ratio between mean background activity and the activity inside the target objects. Two datasets with different CNR_{max} are shown in figure 3. The simulation also exported binary data sets with the correct segmentation, so that the quality of segmentation results of simulated phantom data can be measured more exactly compared to the experimental phantom data sets.

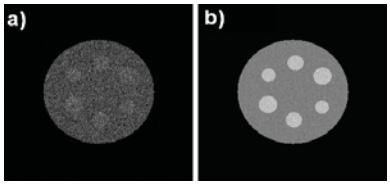

Figure 3: Slice images of simulated phantom data sets evince different contrasts, a) $CNR_{max} = 6.7$, b) $CNR_{max} = 16.6$. Only in b) the target objects are easy to spot.

2.4. Proposed algorithm

The basic idea of using artificial ants for volume segmentation is to define the ants' food source in relation to the grey values in the volume. The ants' group behaviour is a combination of food search (exploration) and food processing (exploitation). The ants communicate only indirectly by a certain kind of stigmergy, namely the process of emitting and interpreting pheromones in the environment. If the ants recognize the target objects, the resulting

pheromone field shows higher pheromone intensity inside positive regions and lower intensity in negative regions. The aim is to generate a pheromone field with this property and use a histogram based threshold algorithm to classify the voxels as correct as possible.

2.4.1. Ants behaviour

ACO approaches are usually implemented as turn based simulations. In every turn all ants are asked for an action, for example moving from position k to position i. The individual ant chooses this action according to the state of its environment. The probability P_{ik} of moving from voxel k to voxel i is, derived from [6], defined as

$$P_{ik} = W(i) / \Sigma_{j/k} W(j).$$

The expression j/k implies that the sum is calculated over all voxels j in the Moore neighbourhood of k. W(j) is equal to the signal intensity in voxel j. This equation results in high probabilities for voxels with high signal. The ants were separated into two castes: scout ants and worker ants. The scouts are assigned to search for valuable food sources, so they consider the activity in the original data set as signal, W(j) = A(j). The principle is visualized in figure 4.

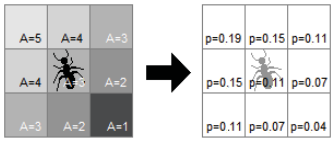

Figure 4: Principle of probability p calculation according to activity A in the 2D Moore neighbourhood of a worker ant.

Worker ants are in charge to move to regions which have been marked with pheromone by scout ants and to intensify the pheromone signal. So the worker ants do not recognize the activity in the original volume, they consider pheromone intensity as signal, W(j) = τ(j). In that way ants of different castes solve two different tasks. After some turns the emergent swarm behaviour can be monitored in the visualisation of the ants' locations, shown in figure 5. The scout ants are initialized continuously while worker ants are generated by reproduction. In every turn scout ants are seeded on 1.3 % of the voxels in the volume on random locations. If the ants fulfil two conditions, they are allowed to reproduce. Reproduction means distributing new worker ants in the neighbourhood of the parent ant. Worker ants appear only by reproduction and scout ant appear only by seeding. The two conditions to be fulfilled by the ants are a) the activity A in the ants voxel in the original volume and b) the pheromone intensity τ must be above specified thresholds A_{min} and τ_{min}. Both thresholds are determined during the ACO simulation dynamically.

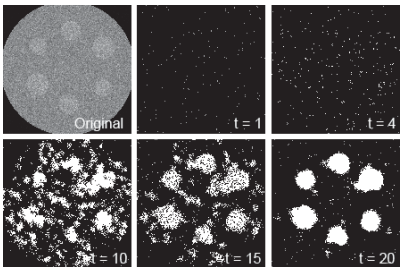

Figure 5: Swarm behaviour shows emergence while processing the ACO simulation on a PET data set (top left). With rising turn count t the worker ants concentrate inside the target objects while scout ants continue exploring the volume.

2.4.2. Pheromone distribution

The pheromone spread inside the volume is characterized by three processes: emission, evaporation and diffusion. Pheromone emission is the process describing the fact, that only ants on voxels with activity above average emit pheromone on the voxel. The mean activity $\bar{A}_t$ of all voxels occupied by ants in turn t is determined and the pheromone to emit $\tau_{e,i,t}$ on voxel i is calculated dependent on the activity A_i :

$$\tau_{e,i,t} = \max(0, A_i - \bar{A}_t)$$

Pheromone evaporation is the process imitating the fact that pheromone disappears with time. The evaporation constant ρ introduced by [6] is used for evaporation and emission of pheromones in one equation. It describes the pheromone $\tau_{i,t+1}$ on voxel i in the next turn (t+1) dependent on pheromone $\tau_{i,t}$ in the current turn t and emitted pheromone $\tau_{e,i,t}$:

$$\tau_{i,t+1} = (1 - \rho)\, \tau_{i,t} + \rho\, \tau_{e,i,t}$$

Pheromone diffusion is the process ensuring that pheromone drifts into regions where no ants are. This is needed because a gradient in every voxel supports ants in orientation in the volume. Diffusion was implemented using a filter which calculates the mean pheromone of the von-Neumann neighbourhood of a voxel k and stores the calculated value in this voxel:

$$\tau'_{k,t} = \Sigma_{j/k}\, \tau_{j,t} / 7$$

To speed up the process of pheromone diffusion the described diffusion process is iterated for five times at the end of every turn. The pheromone field corresponding to the ant distribution shown above is shown in figure 6.

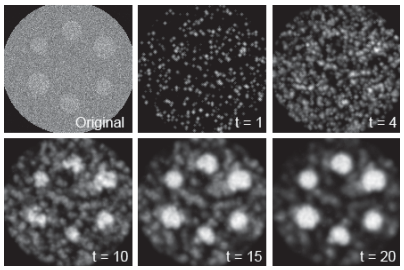

Figure 6: Development of the pheromone field shows target objects more clearly than the original dataset (top left) after an amount t of turns. Light pixels imply high pheromone intensity.

2.4.3. Volume segmentation

The ACO simulation delivers a three dimensional pheromone field for every turn. After simulating a specified amount of turns, special histograms of the pheromone data sets are analysed. The histograms numerate the distribution of the pheromone of all voxels occupied by worker ants. Pheromone is given as relative value τ_{rel} related to the maximum pheromone intensity. Sample histograms and the corresponding ant distribution at different turn counts are shown in figure 7. After ~15 turns the histogram shows two local maxima. The first one ($\tau_{rel} \approx 0.1$) arises from worker ants on the objects perimeter and the second one from worker ants in the objects centre ($\tau_{rel} \approx 0.9$). These two maxima appear because the pheromone gradient, generated by the process of pheromone diffusion, is high inside the object but not on its boundary or in the centre of the object. The final volume segmentation is generated by thresholding the pheromone field of a chosen turn t using a threshold s. Turn t is automatically selected by searching all pheromone histograms having $15 < t < 25$ for the maximum frequency $\max(f_t)$ and choosing the one maximum with the lowest τ_{rel} value. The found τ_{rel} is used as threshold s to segment the pheromone field of turn t in a positive and a negative region.

2.4.4. Experimental setup

Several simulated and experimental phantom datasets were selected for segmentation. Jaccard-Index, sensitivity and specificity of the resulting segmentations are studied in relation to CNR_{max} of the data sets to find a limit of the algorithms variability. All simulated phantom datasets were segmented under equal conditions for five times to evaluate repeatability of the algorithms results. The experimental phantom data set were cut into each six several data sets because the six spheres inside the cylinder showed different CNR_{max} at a single time point. The resulting six datasets were segmented separately.

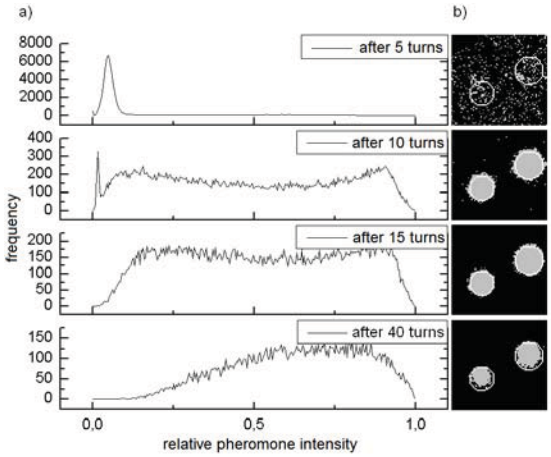

Figure 7: a) Histograms and b) corresponding worker ant distribution (grey). With rising turn count t ants begin to accumulate inside the target objects (white boundary). When ants start to disappear in the perimeter of the objects the first local maximum in the histogram disappears, too.

3. RESULTS

Two test series with each 7 simulated phantom data sets with varying CNR_{max} were generated and segmented five times to evaluate variability of the presented algorithm. The resulting mean quality measurements are shown in figure 8. The corresponding CNR_{max} values are listed in table 1. Successful and failed segmentation processes are shown for comparison in figure 9. If the contrast between target object and background is too low, accumulating worker ants inside the target objects fails. Worker ants continue spreading through the whole cylinder. To predict the algorithms success in segmenting the data sets $CNR_{max} > 11$ was the only observed indicator. The results of segmenting the concerned data sets show Jaccard-Index > 0.7, sensitivity > 0.95 and specificity > 0.99 with low standard deviation between the single results. The fact that algorithms success may be predicted by interpreting CNR_{max} lead to visualizing the resulting quality measurements of the experimental phantom data in relation to CNR_{max}, shown in figure 10. The results of segmenting these two data sets acknowledge the reference CNR_{max} value, because at a specific $CNR_{max} < 11$ the quality measures fall instantly. The other four target objects in phantom data sets could not be segmented successfully. All results of these four objects showed sensitivity < 0.9 or Jaccard-Index < 0.4 indicating segmentation failure.

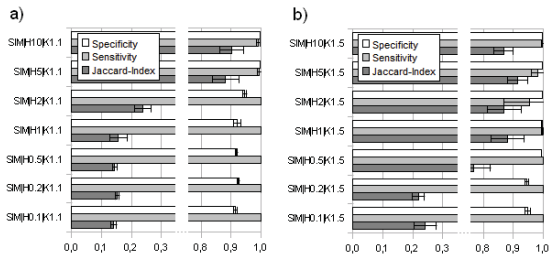

Figure 8: Resulting quality measurements of simulated phantom data sets

Table 1: Contrast-to-noise-ratios of simulated phantom data sets

Data set	CNR_{max}	Data set	CNR_{max}
SIM|H10|K1.1	12.12	SIM|H10|K1.5	38.78
SIM|H5|K1.1	10.12	SIM|H5|K1.5	30.16
SIM|H2|K1.1	8.20	SIM|H2|K1.5	19.91
SIM|H1|K1.1	7.15	SIM|H1|K1.5	16.23
SIM|H0.5|K1.1	8.50	SIM|H0.5|K1.5	15.47
SIM|H0.2|K1.1	7.18	SIM|H0.2|K1.5	10.87
SIM|H0.1|K1.1	5.93	SIM|H0.1|K1.5	10.33

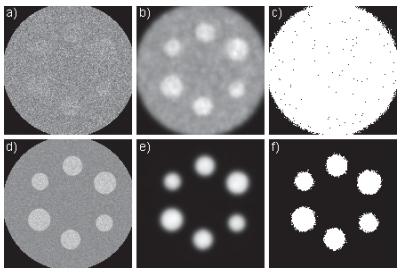

Figure 9: Comparison of the ACO simulation in a successful segmentation process and a failed process. The slice images of the simulation on the data sets SIM|H0.1|K1.1 (top) and SIM|H0.5|K1.5 (bottom), a,d) original data set, b,e) pheromone field after 20 turns, c,f) distribution of worker ants after 20 turns.

Repeatability was measured by comparison of single results after segmenting identical data sets using Jaccard-Index. Five separately generated segmentation results are shown in figure 11. Comparing them pairwise using the Jaccard-Index results in the values shown in Table 2. The results are repeatable, indicated by a Jaccard-Index > 0.9. But compared to the correct segmentation they show Jaccard-Index ≈ 0.57, sensitivity ≈ 0.87 and specificity ≈ 0.99. Repeatability of segmentation of the simulated phantom data sets was also analysed. The mean Jaccard-Index of pair wise comparison of separately generated results was always above 0.8 and ranged up to 0.98. These high Jaccard-Index values indicate that segmentation results are repeatable even if the segmentation failed.

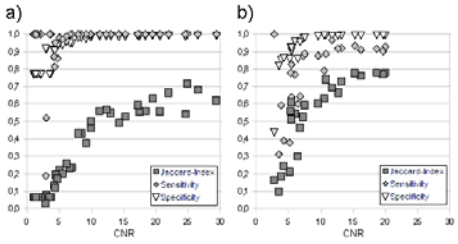

Figure 10: Quality measures of results of segmenting experimental phantom data sets plotted above CNR_{max} of a) a glass sphere and b) a wax sphere. At a specific $CNR_{max} < 11$ the quality measures fall instantly. When $CNR_{max} > 11$ the quality measures imply segmentation success.

Figure 11: Slice image of a wax sphere of the experimental phantom data set (CNR_{max} = 9.54) with five separately generated segmentation results (black boundary) displayed over correct segmentation (white boundary).

Table 2: Resulting Jaccard-Index values after pair wise comparison of segmentation results.

Data set	2	3	4	5
1	0.92	0.91	0.91	0.91
2		0.99	0.98	0.96
3			0.99	0.95
4				0.95

4. DISCUSSION

The presented segmentation algorithm is implemented as a combination of an ACO simulation and a histogram based threshold segmentation algorithm. The resulting pheromone field of the ACO simulation shows the target objects with an easier to delineate boundary than in the original data sets. But this fact is only valid if the contrast of the original data set is high enough to make the ants successful in differentiating voxels of the target object and voxels of the background. All processed data sets with a $CNR_{max} > 11$ could be segmented. Other contrast measures, like the ratio between mean activity in target object and background volume, were examined but delivered no grounds for a presumption of segmentation success. Simulated phantom data sets with various ratios between mean activity in target and background were segmented adequately using the proposed algorithm as long as the CNR_{max} was high enough. So only $CNR_{max} > 11$ serves as approximate reference value to predict segmentation success. It is an experiential value and it is not expected to be universally valid.

All successful segmentations of simulated phantom data sets showed a Jaccard-Index > 0.75, sensitivity > 0.95 and specificity > 0.99. But especially specificity must be regarded carefully. High specificity values do not necessarily imply segmentation success because specificity is related to the amount of real negative voxels. To underline this fact, the amount of real negative voxels n_n and the amount of real positive voxels n_p of the simulated phantom data sets are given:

$$n_n = 1928398$$
$$n_p = 37682$$

Assumptive a segmentation process classified all positive voxels correct ($n_{tp} = n_p$) and another equal amount of real negative voxels have been classified positive ($n_{fp} = n_p$, $n_{tn} = n_n - n_p$), the specificity of this segmentation result is

$$SP = n_{tn} / (m_{tn} + m_{fp}) = (m_n - m_p) / m_n$$
$$= (1928398 - 37682) / 1928398$$
$$= 0.98$$

A high specificity value of 0.98 suggests a successful segmentation process but the Jaccard-Index (in this example 0.5) shows that the process in this case failed. When analysing segmentation quality measurements always the combination of several measures must be regarded. A single value of the presented measures is not able to value the segmentation quality.

The proposed method was not able to segment all experimental phantom data sets even if the data sets showed a sufficient high CNR_{max} value. The reason for this failure must be seen in the inhomogeneous distribution of activity inside the wax spheres. Sub volumes within the spheres showing high signal resulted from agglutinating Gallium while stirring a Gallium-Acetone solution together with hot wax. Sub volumes showing low signal came up during cooling process of the spheres inside the refrigerator. The failure of the method in segmenting such objects must be considered positively, because the algorithm is thought to segment objects with signal above the average and the target objects partly show no signal above average.

The high repeatability of the generated results suggests that the method should be developed further to handle patient datasets. One issue is to handle more complicated test data sets. For illustration the algorithm was applied on a data set with an inhomogeneous background volume and a complicated target object. The resulting pheromone field and worker ant distribution is shown in figure 12. The method is able to segment the data set, but some single worker ants in the top right corner are segmenting a target object which does not exist. At this point the algorithm must be improved.

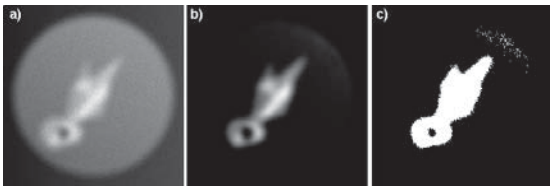

Figure 12: ACO simulation applied on a more complicated test data set. a) Original data, b) pheromone field after 12 iterations, c) distribution of worker ants after 12 iterations

5. CONCLUSION

The overall results of the proposed algorithm serve as proof of concept. It is possible to use artificial ants operating in image space and generating a pheromone field where the target object can be segmented more clearly than in the original data set. If the contrast measure CNR_{max} of the original PET data set is above 11 the method allows delineation of test objects with homogeneously distributed activity with sensitivity > 0.95, specificity > 0.99 and a Jaccard-Index > 0.75 from a homogeneously distributed background volume. The next step will be improving the algorithm to allow segmentation of patient data sets with high repeatability and as independent of contrast as possible.

6. REFERENCES

1. Hockel, M., et al., *Intratumoral pO2 predicts survival in advanced cancer of the uterine cervix.* Radiother Oncol, 1993. **26**(1): p. 45-50.
2. Nehmeh, S.A., et al., *Reproducibility of intratumor distribution of (18)F-fluoromisonidazole in head and neck cancer.* Int J Radiat Oncol Biol Phys, 2008. **70**(1): p. 235-42.
3. Marco, D., *Ant Algorithms Solve Difficult Optimization Problems*, in *Proceedings of the 6th European Conference on Advances in Artificial Life*. 2001, Springer-Verlag.
4. Colorni, A., M. Dorigo, and V. Maniezzo. *Distributed Optimization by Ant Colonies*. in *European Conference on Artificial Life*. 1992.
5. Huang, P., H. Cao, and S. Luo, *An artificial ant colonies approach to medical image segmentation.* Comput Methods Programs Biomed, 2008. **92**(3): p. 267-73.
6. Chialvo, D. and M.M. Millonas, *How Swarms Build Cognitive Maps*, in *The Biology and Technology of Intelligent Autonomous Agents*, L. Steels, Editor. 1995. p. 439-450.